

Near-Infrared to Visible Light-Upconversion in Molecules: From Dream to Reality

Yan Suffren,^{‡,||} Davood Zare,^{‡,||} Svetlana V. Eliseeva,[‡] Laure Guénée,[§] Homayoun Nozary,[†] Timothée Lathion,[†] Lilit Aboshyan-Sorgho,[†] Stéphane Petoud,^{‡,*} Andreas Hauser,^{‡,*} and Claude Piguet^{‡,*}

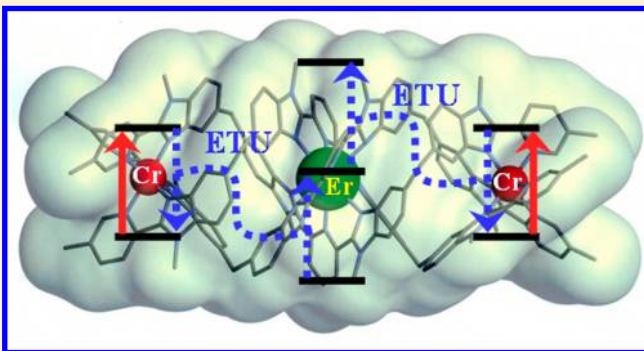
[†]Department of Inorganic and Analytical Chemistry and [‡]Department of Physical Chemistry, University of Geneva, 30 quai E. Ansermet, CH-1211 Geneva 4, Switzerland

[§]Laboratory of Crystallography, University of Geneva, 24 quai E. Ansermet, CH-1211 Geneva 4, Switzerland

^{||}Centre de Biophysique Moléculaire and Le STUDIUM Institute for Advanced Studies, Region Centre, CNRS UPR 4301, Rue Charles Sadron, F-45071 Orléans Cedex 2, France

S Supporting Information

ABSTRACT: Light-upconversion via stepwise energy transfer from a sensitizer to an activator exploits linear optics for converting low-energy infrared or near-infrared incident photons to higher energy emission. This approach is restricted to activators possessing intermediate long-lived excited states such as those found for trivalent lanthanide cations dispersed in solid-state matrices. When the activator is embedded in a molecular complex, efficient nonradiative relaxation processes usually reduce excited state lifetimes to such an extent that upconversion becomes too inefficient to be detected under practical excitation intensities. Theoretical considerations presented here predict that the combination of at least two millisecond time scale sensitizers with a central lanthanide activator in supramolecular complexes circumvents this bottleneck by creating a novel upconversion pathway, in which successive excitations are stored on the sensitizers prior to inducing stepwise energy transfer processes. Application of this concept to the chromium/erbium pair demonstrates that strong-field trivalent chromium chromophores irradiated with near-infrared photons produce upconverted green erbium-centered emission in discrete dinuclear and trinuclear triple-stranded helicates.



■ INTRODUCTION AND THEORETICAL BACKGROUND

Stimulated by the need for materials possessing efficient near-infrared to visible light upconversion processes for solar cell technology¹ and for in situ biological probes and sensors,² we present here a rigorous and simple theoretical model for pushing the limits of miniaturization beyond solid-state nanoparticles and polymers with the design of upconverting molecular entities. Luminescent systems based on a single chromophore usually follow the well-known principle first formulated by Stokes, which states that emitted photons possess lower energy than the ones used for the excitation. The induction of anti-Stokes emission was thus limited for a long time to the thermal population of states by a few quanta kT of energy above the ground state, a phenomenon familiar to Raman spectroscopists. The rational violation of this principle via the sequential absorption of two infrared (IR) excitation photons to reach an excited state the emission energy of which exceeds the incident radiation by 10–100 times kT , a phenomenon often referred to as superexcitation or excited state absorption (ESA), was only established during the early 1960s with the help of open-shell trivalent lanthanides for the design of a detector called an “infrared quantum counter” (IRQC).^{3,4} Solving the standard set of linear differential

equations, eqs 1 and 2, relevant to the diagram modeling the activator-centered one ion ESA mechanism depicted in Figure 1a (see Appendix 1 in Supporting Information for details) yields the steady-state normalized population densities $N^{(i)}$ of Figure 1b obtained under continuous-wave irradiation at increasing pump intensities. The pumping rate constant $k_A^{\text{exc}(i \rightarrow j)}$ is given by eq 3, where λ_p is the pump wavelength, P is the incident pump intensity, $\sigma_A^{j \rightarrow i}$ is the absorption cross section of the activator-centered $i \rightarrow j$ transition, h is the Planck constant, and c is the vacuum speed of light.⁵

$$\begin{pmatrix} \frac{dN^{(0)}}{dt} \\ \frac{dN^{(1)}}{dt} \\ \frac{dN^{(2)}}{dt} \end{pmatrix} = \begin{pmatrix} -k_A^{\text{exc}(0 \rightarrow 1)} & k_A^{1 \rightarrow 0} & k_A^{2 \rightarrow 0} \\ k_A^{\text{exc}(0 \rightarrow 1)} & -(k_A^{1 \rightarrow 0} - k_A^{\text{exc}(1 \rightarrow 2)}) & k_A^{2 \rightarrow 1} \\ 0 & k_A^{\text{exc}(1 \rightarrow 2)} & -(k_A^{2 \rightarrow 0} + k_A^{2 \rightarrow 1}) \end{pmatrix} \times \begin{pmatrix} N^{(0)} \\ N^{(1)} \\ N^{(2)} \end{pmatrix} \quad (1)$$

Received: October 31, 2013

Revised: November 25, 2013

Published: December 12, 2013

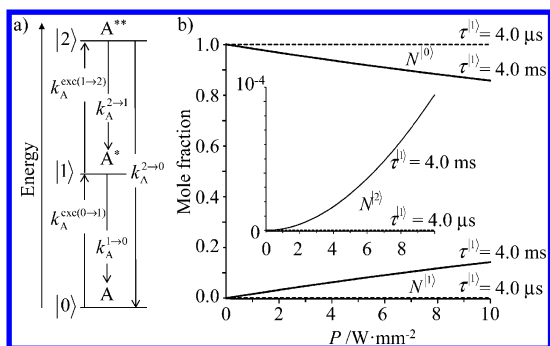


Figure 1. (a) Kinetic scheme depicting the modeling of the one ion excited state absorption (ESA) process occurring upon off-resonance irradiation into the activator-centered absorption bands, where $k_A^{(1 \rightarrow 0)}$ stands for the global decay rate constant of the first A^* excited state and $(k_A^{(2 \rightarrow 1)} + k_A^{(2 \rightarrow 0)})$ similarly applies for the second A^{**} excited state. (b) Normalized steady-state population densities for the various levels at increasing incident pump intensity for a standard erbium activator computed by using $\lambda_p = 750 \text{ nm}$,⁶ absorption cross sections $\sigma_A^{0 \rightarrow 1} \approx \sigma_A^{1 \rightarrow 2} = 10^{-24} \text{ m}^2$, $k_A^{(2 \rightarrow 0)} = (\tau_{\text{Er}, \text{rad}}^{4\text{S}_{3/2}})^{-1} = (619 \text{ } \mu\text{s})^{-1}$, $k_A^{(2 \rightarrow 1)} = (\tau_{\text{Er}}^{4\text{F}_{3/2}})^{-1} = (16 \text{ } \mu\text{s})^{-1}$.⁸ The full traces correspond to slow-relaxing erbium(III) doped into yttrium–aluminum–garnet (YAG) with $k_A^{1 \rightarrow 0} = (\tau_{\text{Er}}^{4\text{I}_{3/2}})^{-1} = (4.0 \text{ ms})^{-1}$,⁹ whereas the dotted traces stand for a fast-relaxing erbium(III) coordination complex with $k_A^{1 \rightarrow 0} = (\tau_{\text{Er}}^{4\text{I}_{3/2}})^{-1} = (4.0 \text{ } \mu\text{s})^{-1}$.¹⁰ The 0 – 10^{-4} normalized population density range used for $N^{(2)}$ is highlighted in the inset.

$$N_{\text{tot}} = N^{(0)} + N^{(1)} + N^{(2)} = 1 \quad (2)$$

$$k_A^{\text{exc}(i \rightarrow j)} = \frac{\lambda_p}{hc} P \sigma_A^{i \rightarrow j} = f P \sigma_A^{i \rightarrow j} \quad (3)$$

Since the intensity of the targeted upconverted emission is proportional to the normalized population density of the second excited state A^{**} ($N^{(2)}$ in eqs 1 and 2), the inset of Figure 1b demonstrates that a short intrinsic lifetime of the intermediate excited state A^* indeed has a deleterious effect on $N^{(2)}$ based on the one ion ESA mechanism.^{6–10} Consequently, applications of lanthanide-centered upconversion for improving solar cell efficiencies¹¹ or for the induction of photobiological processes under deeply penetrating NIR irradiation¹² systematically rely on comparatively long-lived erbium(III) or thulium(III)-containing miniaturized solids. Doped garnet nanoparticles are currently exploited for this purpose despite the limited control over their synthesis, while short-lived molecular systems have generally been dismissed.^{13,14}

In 1966, Auzel introduced the APTE concept (“*addition de photon par transfert d’énergie*”), later termed “energy transfer upconversion” (ETU),⁴ in which the ineffective direct pumping into the parity forbidden intrashell f–f electric dipolar transitions of trivalent lanthanide cations is replaced by the excitation of sensitizers possessing larger absorption cross sections, followed by sequential energy transfer processes, eventually leading to the multistep excitation of the activator (Figure 2a). With such a strategy, the drastic consequences of activators with too short intermediate excited-state lifetimes can be partially overcome by the use of long-lived excited sensitizers (S^*). Comparison of Figures 1a and 2a immediately shows that the overall intensity of steady-state upconverted emitted light with the ETU mechanism roughly gains by a factor of $(W^{S \rightarrow A})^2 (N_S^{(0)})^2 (\sigma_A^{0 \rightarrow 1})^2 / (\sigma_A^{1 \rightarrow 2})$ over one ion ESA,⁴ whereby $W^{S \rightarrow A}$ is the probability of the intermolecular sensitizer to activator energy transfer (second-order rate constant) and $N_S^{(0)}$ is the concentration of the sensitizer.¹⁵

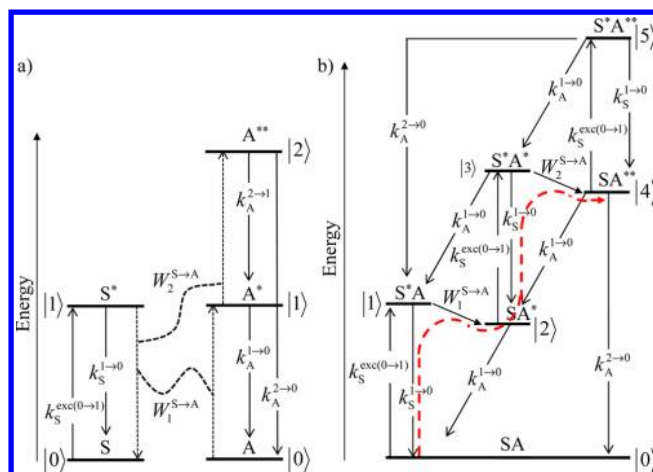


Figure 2. Kinetic schemes depicting the modeling of energy transfer upconversion (ETU) processes occurring upon off-resonance irradiation into the sensitizer-centered absorption bands in (a) a statistically doped S/A solid and (b) a discrete SA dinuclear molecule. $k_S^{\text{exc}(0 \rightarrow 1)}$ is the pumping rate constant for irradiation into the sensitizer absorption band (eq 3), $k_S^{i \rightarrow j}$ and $k_A^{i \rightarrow j}$, respectively, are the decay rate constants (i.e., the sum of radiative and nonradiative processes) of level i into level j centered on the sensitizer and on the activator, respectively, and $W_n^{S \rightarrow A}$ are the rate constants of sensitizer-to-activator energy transfer processes. The red dashed pathway highlights the activator-centered mechanism responsible for ETU in a dinuclear SA complex.

Consequently, solid-state garnets or nanoparticles containing Er(III), Tm(III), or Pr(III) activators are regularly codoped with Yb(III) sensitizers, the unique near-infrared long-lived $^2\text{F}_{5/2}$ excited state of which is exploited as a relay in ETU.¹⁶

In discrete lanthanide coordination complexes, one ion ESA-based upconversion has been achieved with very limited success,¹⁷ while the alternative ETU mechanism combining a lanthanide activator with long-lived sensitizers has been hypothesized only once without experimental support.¹⁸ The favorable influence of a high concentration of sensitizer through the factor $(N_S^{(0)})^2$ for ETU processes is only valid for systems with independent sensitizers and activators, a condition which is only met in statistically doped solids (Figure 2a).¹⁵ When the sensitizer is associated with an activator in a discrete SA molecule, the correlation between the two partners transforms the gain of ETU over one ion ESA to $(W^{S \rightarrow A})^2 (\sigma_S^{0 \rightarrow 1})^2 / (\sigma_A^{0 \rightarrow 1} \sigma_A^{1 \rightarrow 2})$ where $W^{S \rightarrow A}$ is now the first-order rate constant for the intramolecular sensitizer to activator energy transfer. Moreover, the short lifetime of the activator-centered intermediate excited SA^* level in an isolated molecular complex becomes again a major drawback for the upconversion, irrespective of the intrinsic lifetime of the sensitizer excited state (level |2> in Figure 2b).

The situation changes completely with the introduction of a second long-lived sensitizer per activator in a SAS triad (Figure 3a). Beyond the expected statistical gain of a factor $2^2 = 4$ for the activator-centered ETU mechanism resulting from the doubling of the number of sensitizers (red paths in Figures 2b and 3a), the presence of two sensitizers in the same complex opens an unprecedented sensitizer-centered pathway (green path in Figure 3a). Two successive excitation processes providing the doubly excited S^*AS^* level (level |4> in Figure 3a), are followed by two successive $S \rightarrow A$ energy transfer steps leading to the targeted upconverted emission. The latter mechanism is much less sensitive to the excited-state lifetime of the activator. The normalized steady-state population densities computed for

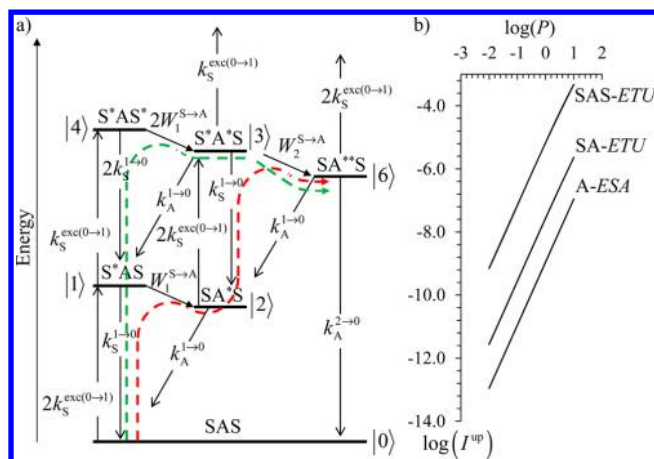


Figure 3. (a) Low-energy part of the kinetic scheme for modeling energy transfer upconversion (ETU) occurring upon off-resonance irradiation into the sensitizer-centered absorption bands of a discrete SAS triad (Figures S1–S2 in the Supporting Information contain the complete kinetic scheme). The red (A-centered) and green (S-centered) dashed pathways highlight the two possible mechanisms responsible for ETU. (b) Comparison of the computed quadratic dependence of the A-centered upconverted emission intensities (I^{up}) on the incident pump intensity (P in W/mm^2) for the molecular fast-relaxing erbium activator of Figure 1 ($k_A^{1 \rightarrow 0} = (4.0 \mu\text{s})^{-1}$), undergoing either one ion ESA (A-ESA, $\sigma_A^{0 \rightarrow 1} \approx \sigma_A^{0 \rightarrow 2} = 10^{-24} \text{ m}^2$) or indirect sensitizations in dinuclear (SA-ETU) and trinuclear complexes (SAS-ETU, $\sigma_S^{0 \rightarrow 1} = 10^{-23} \text{ m}^2$) by using $k_S^{1 \rightarrow 0} = (1.0 \text{ ms})^{-1}$ and $\eta(W^{S \rightarrow A}) = 50\%$.

the doubly excited states A^{**} of a fast-relaxing erbium(III) activator combined with millisecond long-lived sensitizers in molecules allows to predict an improvement in the intensity of the upconverted emission of up to 2 orders of magnitude upon

switching from a dinuclear SA complex (exclusive operation of the activator-centered ETU) into a trinuclear SAS complex (concomitant operation of activator- and sensitizer-centered ETUs), whereas the efficiency of the alternative one ion ESA remains marginal (Figure 3b).

RESULTS AND DISCUSSIONS

Building on our experience in designing heterometallic Cr/Ln supramolecular complexes, in which trivalent chromium ions, Cr(III), act as millisecond-range sensitizers for trivalent lanthanides Ln(III),¹⁹ we prepared a series of isostructural trinuclear dimetallic triple-stranded $[\text{MLnM}(\text{L1})_3](\text{CF}_3\text{SO}_3)_9$ helicates (further termed MLnM) with $M = \text{Ga(III)}$ or Cr(III) and $\text{Ln} = \text{Y(III)}$ or Er(III) (Appendix 2). All complexes were characterized by satisfactory elemental analysis (Table S1). X-ray diffraction studies performed on single crystals demonstrate isostructurality in the solid state (Table 1) together with the formation of triple-stranded helical cations $[\text{MLnM}(\text{L1})_3]^{9+}$ (Figure 4a).²⁰ Their kinetic inertness and persistence in solution at (sub)millimolar concentrations in acetonitrile solution were established by electrospray-ionization mass spectrometry (ESI-MS, Table S2) and proton nuclear magnetic resonance (^1H NMR, Figures S3 and S4).¹⁸

The diamagnetic closed-shell GaYGa complex is used as a reference for the location of the energies of the broad singlet ($^1\pi^*$) and triplet ($^3\pi^*$) ligand-centered excited states in absence of metal-centered photophysical activity (Figures 5a and S5). Detailed photophysical studies of GaErGa (pure complexes or diluted at 2–10% in GaYGa) provide information on the electronic structure of the nine-coordinate Er(III) N_9 chromophore (Figures 5c), while the investigation of CrYCr delivers the corresponding information for the strong-field six-coordinate

Table 1. Summary of Crystal Data for $[\text{CrLnCr}(\text{L1})_3]_2(\text{CF}_3\text{SO}_3)_{18}(\text{C}_3\text{H}_5\text{N})_{30}$ ($\text{Ln} = \text{Eu, Y, Er}$) and $[\text{GaLnGa}(\text{L1})_3]_2(\text{CF}_3\text{SO}_3)_{18}(\text{C}_3\text{H}_5\text{N})_{30}$ ($\text{Ln} = \text{Y, Er}$)^a

	CrLnCr		
	CrEuCr ^a	CrErCr	CrYCr
empirical formula	$\text{C}_{414}\text{H}_{408}\text{Cr}_4\text{Eu}_2$ $\text{F}_{54}\text{N}_{96}\text{O}_{54}\text{S}_{18}$	$\text{C}_{414}\text{H}_{408}\text{Cr}_4\text{Er}_2$ $\text{F}_{54}\text{N}_{96}\text{O}_{54}\text{S}_{18}$	$\text{C}_{414}\text{H}_{408}\text{Cr}_4\text{Y}_2$ $\text{F}_{54}\text{N}_{96}\text{O}_{54}\text{S}_{18}$
formula weight	9707.26	9737.86	9581.15
temperature, K	100(2)	150(2)	150(2)
wavelength, Å	0.70000	1.5418 Å	1.5418 Å
crystal system, space group	monoclinic, $P2_1/c$	monoclinic, $P2_1/c$	monoclinic, $P2_1/c$
unit cell dimensions	$a = 29.3890(4)$ Å $b = 61.0950(10)$ Å $c = 26.6462(3)$ Å $\beta = 99.375(2)^\circ$	$a = 29.3619(5)$ Å $b = 60.379(2)$ Å $c = 26.6897(3)$ Å $\beta = 98.635(1)^\circ$	$a = 29.3565(7)$ Å $b = 60.464(2)$ Å $c = 26.6469(4)$ Å $\beta = 98.675(2)^\circ$
vol, Å ³	47204.8(11)	46780(2)	46757(2)
	GaLnGa		
	GaYGa	GaErGa	
empirical formula	$\text{C}_{414}\text{H}_{408}\text{Ga}_4\text{Y}_2\text{F}_{54}\text{N}_{96}\text{O}_{54}\text{S}_{18}$	$\text{C}_{414}\text{H}_{408}\text{Ga}_4\text{Er}_2\text{F}_{54}\text{N}_{96}\text{O}_{54}\text{S}_{18}$	
formula weight	9652.06	9444.77	
temperature, K	150(2)	150(2)	
wavelength, Å	1.5418	1.5418	
crystal system, space group	monoclinic, $P2_1/c$	monoclinic, $P2_1/c$	
unit cell dimensions	$a = 29.3656(5)$ Å $b = 60.179(2)$ Å $c = 26.7184(5)$ Å $\beta = 98.801(2)^\circ$	$a = 29.3602(5)$ Å $b = 61.334(2)$ Å $c = 26.7917(2)$ Å $\beta = 98.955(1)^\circ$	
vol, Å ³	46661(2)	47658(2)	

^aThe complete crystal structures were solved for CrEuCr and CrYbCr using synchrotron radiation¹⁸ and for GaYGa using Cu $K\alpha$ radiation.²⁰

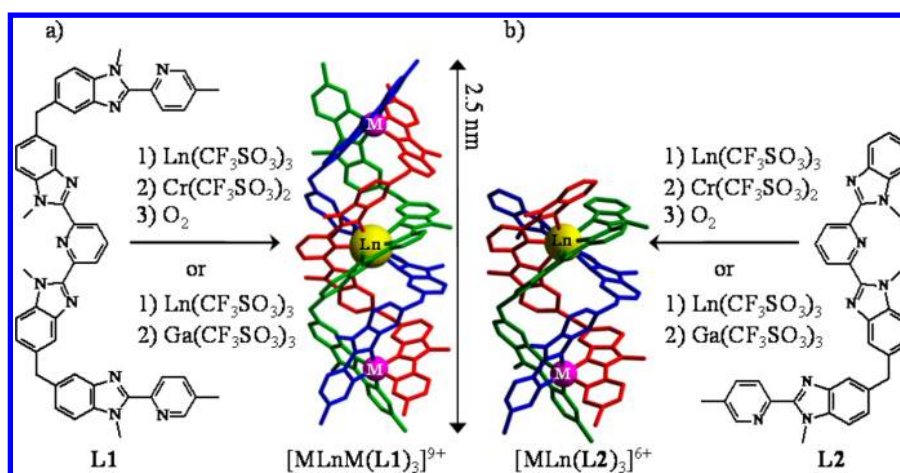


Figure 4. Syntheses and molecular structures of the triple-stranded (a) trinuclear $[MLnM(L1)_3]^{9+18,20}$ and (b) dinuclear $[MLn(L2)_3]^{6+}$ complexes for $M = Cr, Ga$ and $Ln = Y, Er$.²¹

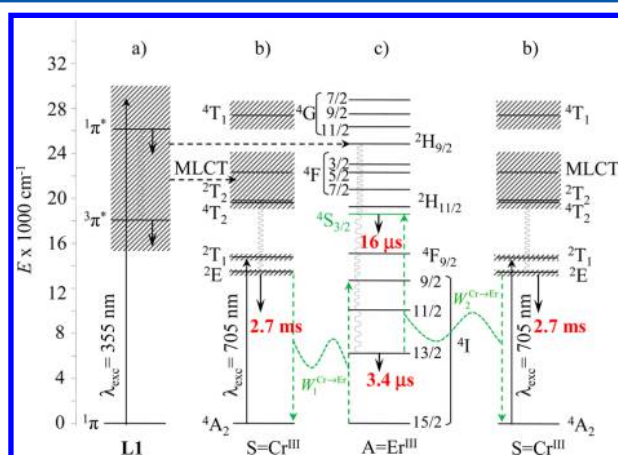


Figure 5. Jablonski diagrams obtained from absorption and emission spectra recorded for the different chromophores in $[CrErCr(L1)_3]-(CF_3SO_3)_9$: (a) L1, (b) $[CrN_6]$, and (c) $[ErN_9]$ (see Appendix 3 for details). The Cr-centered and Er-centered downshifted emission obtained upon ligand-centered excitation at 355 nm in $CrErCr$ is shown on the left (excitation = full upward arrows, internal conversion = curled down lines, energy transfer = dotted black arrows, emission = full downward arrows), whereas the upconversion emission produced by Cr-centered excitation at 705 nm is depicted on the right (ETU = dotted green arrows). Relevant intrinsic luminescence lifetimes at 10 K for the emissive metal-centered levels in $CrYCr$ and $GaErGa$ are given in red.

$Cr(III)N_6$ sites (Figures 5b). Briefly, the excitation into the ligand-centered $^1\pi^* \leftarrow ^1\pi$ transitions at 355 nm ($\tilde{\nu}_{exc} = 28169 \text{ cm}^{-1}$) results in downshifted luminescence for both $GaErGa$ and $CrYCr$. In the first case, partial energy transfer onto $Er(III)$ eventually leads to residual broad ligand-centered emission ($^1\pi^* \rightarrow ^1\pi$) combined with narrow band Er-centered $Er(^4S_{3/2} \rightarrow ^4I_{15/2})$ and $Er(^4I_{13/2} \rightarrow ^4I_{15/2})$ luminescence in the green at 542 nm (18450 cm^{-1}) and near-infrared (at 1545 nm or 6470 cm^{-1}), respectively, as previously reported for the $ZnErZn$ helicate (Figure S6).^{18,19} For $CrYCr$, almost quantitative energy transfer onto trivalent chromium produces the typical narrow band originating from the long-lived spin-flip $Cr(^2E \rightarrow ^4A_2)$ transition and occurring in the near-infrared at 750 nm (13330 cm^{-1} , Figure S7). The Jablonski diagrams gathered in Figure 5 summarize the energies of the ground and excited states pertinent for each chromophore in these supramolecular complexes (see Appendix 3 in Supporting Information for details).¹⁵

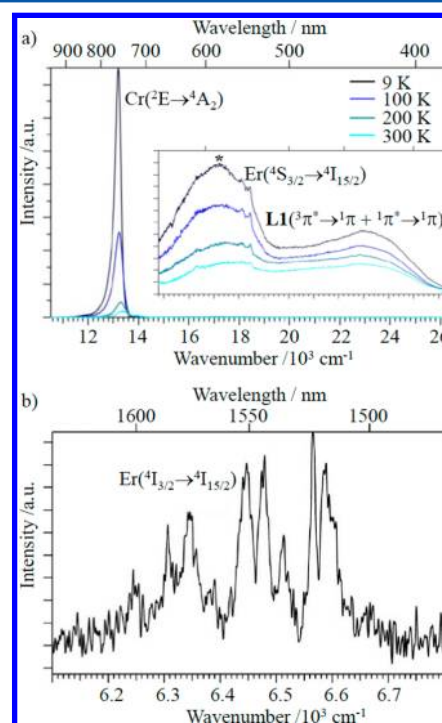


Figure 6. (a) Visible to near-infrared ($\tilde{\nu}_{exc} = 28169 \text{ cm}^{-1}$ or $\lambda_{exc} = 355 \text{ nm}$, the inset shows a magnification of the $15000\text{--}26000 \text{ cm}^{-1}$ domain) and (b) visible to far near-infrared ($\tilde{\nu}_{exc} = 24690 \text{ cm}^{-1}$ or $\lambda_{exc} = 405 \text{ nm}$) solid-state emission spectra of $[CrErCr(L1)_3](CF_3SO_3)_9$ at various temperatures recorded under ligand-centered excitations. (*) Residual fluorescence signal arising from the sample holder under UV irradiation.

In the target $CrErCr$ complex, ligand-centered excitation at 355 or 405 nm is followed by energy transfer onto both metallic chromophores leading to the simultaneous downshifted green $Er(^4S_{3/2} \rightarrow ^4I_{15/2})$ (542 nm, 18450 cm^{-1}), and near-infrared $Cr(^2E \rightarrow ^4A_2)$ (750 nm, 13330 cm^{-1}) and $Er(^4I_{13/2} \rightarrow ^4I_{15/2})$ (1545 nm, 6470 cm^{-1}) emissions (Figures 6 and S8). Compared with $CrYCr$, the additional intramolecular intermetallic $Cr(^2E) \rightarrow Er(^4I_{9/2})$ energy transfer operating in $CrErCr$ ($W_1^{Cr \rightarrow Er}$ in Figure 5) reduces the $Cr(^2E)$ excited-state lifetimes by approximately 30% (Table S3). Considering the intrinsic decay rates constant $k_{Cr}^{1 \rightarrow 0} = (\tau_{Cr}^2)^{-1}$ found for the $Cr(^2E)$ levels in $CrYCr$ (in absence of an activator) and the observed decay rate constant in

CrErCr (in presence of the activator) gives values of $W_1^{\text{Cr} \rightarrow \text{Er}} \approx 100\text{--}200 \text{ s}^{-1}$ for the rate constants of the energy transfer processes (eq 4) and $\eta_1^{\text{Cr} \rightarrow \text{Er}} \approx 25\text{--}35\%$ for their efficiencies (eq 5) for temperatures in the range of 5–250 K (Table S3).¹⁹ Interestingly, these two parameters do not significantly depend on the dilution of the active CrErCr complex into inactive GaYGa (solid-state) or into propionitrile/acetonitrile mixtures (solution), a behavior supporting the exclusive operation of intramolecular Cr \rightarrow Er energy transfer processes.

$$W_1^{\text{Cr} \rightarrow \text{Er}} = k_{\text{Cr}}^{\text{obs}}(\text{CrErCr}) - k_{\text{Cr}}^{1 \rightarrow 0}(\text{CrYCr}) \quad (4)$$

$$\eta_1^{\text{Cr} \rightarrow \text{Er}} = 1 - k_{\text{Cr}}^{1 \rightarrow 0}(\text{CrYCr})/k_{\text{Cr}}^{\text{obs}}(\text{CrErCr}) \quad (5)$$

Though modest, the rate constants obtained for the Cr \rightarrow Er energy transfer processes occurring in CrErCr are in line with previous studies involving a Cr(²E) donor separated by 8–10 Å from various lanthanide acceptors in absence of a short bridge between the metals.¹⁹ In these conditions, the poor spectral overlap resulting from the narrow Cr-centered emission and Er-centered absorption bands limits the efficiency of energy transfer processes mediated by multipolar electrostatic interactions (i.e., Förster-type energy transfer).¹⁵

Continuous-wave near-infrared (NIR) irradiation of the sensitizer into its Cr(²E \leftarrow ⁴A₂) (742 nm) or Cr(²T₁ \leftarrow ⁴A₂) (705 nm) transitions in CrErCr produces downshifted millisecond Cr-centered emission at 750 nm (Figure 7, blue trace),

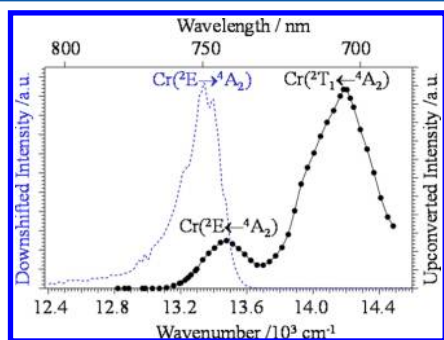


Figure 7. Black full trace: excitation spectrum of the green upconverted Er(⁴S_{3/2} \rightarrow ⁴I_{15/2}) emission in [CrErCr(L1)](CF₃SO₃)₉ (10% doped in GaYGa, solid-state, 31 K, $P = 20$ mW loosely focused onto the sample). The dotted blue trace refers to the downshifted Cr(²E \rightarrow ⁴A₂) phosphorescence obtained upon ligand-centered excitation ($\tilde{\nu}_{\text{exc}} = 28169 \text{ cm}^{-1}$ or $\lambda_{\text{exc}} = 355 \text{ nm}$).

together with a NIR Er(⁴I_{13/2} \rightarrow ⁴I_{15/2}) emission at 1545 nm induced by the Cr(²E) \rightarrow Er(⁴I_{9/2}) energy transfer. As expected, the apparent lifetime of the Er(⁴I_{13/2} \rightarrow ⁴I_{15/2}) emission, which occurs in the microsecond range in GaErGa, now mirrors that of the long-lived feeding Cr(²E) level and extends to the millisecond range for CrErCr (Table S4).¹⁹ In line with preliminary measurements,¹⁸ near-infrared irradiation in the Cr(²E, ²T₁)-centered feeding levels also reveals an upconverted green emission corresponding to the Er(⁴S_{3/2} \rightarrow ⁴I_{15/2}) transition at 542 nm (Figure 7, black trace), which is detected in the 5–293 K range for CrErCr samples in solution (acetonitrile:propionitrile 4:1, Figure 8a, top dark green trace) and in the solid state (as pure complex or diluted at 2–10% in GaYGa, Figures S9–S14). In order to identify the excitation mechanism, the intensity of the upconverted Er(⁴S_{3/2} \rightarrow ⁴I_{15/2}) emission I^{up} was recorded at increasing laser pumping intensities P . Plots of $\log(I^{\text{up}})$ versus $\log(P)$ are linear at reasonable pumping

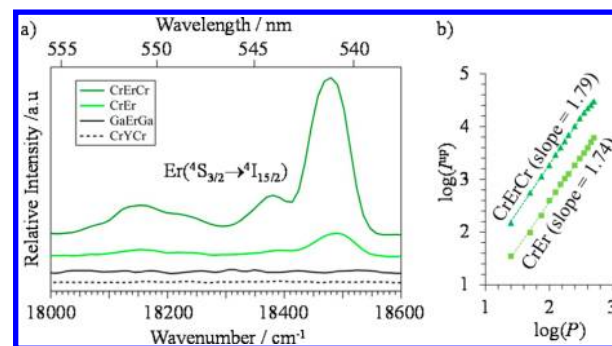


Figure 8. (a) Green upconverted Er(⁴S_{3/2} \rightarrow ⁴I_{15/2}) emission observed for [CrErCr(L1)](CF₃SO₃)₉ and [CrEr(L2)](CF₃SO₃)₆ in solution (10 mM in acetonitrile:propionitrile (4:1), 31 K, $\tilde{\nu}_{\text{exc}} = 13986 \text{ cm}^{-1}$ or $\lambda_{\text{exc}} = 715 \text{ nm}$, $P = 100$ mW loosely focused onto the sample). For direct comparison background spectra obtained with the inert reference CrYCr and GaErGa systems are included. (b) Upconverted emission intensity (I^{up}) with respect to incident pump intensity into the Cr(²T₁ \leftarrow ⁴A₂) transition (P in mW) for CrErCr and CrEr on a log–log plot, symbols: experimental points; lines: linear fits.

intensities with slopes in the range 1.65–1.93 corresponding to $n = 2$ -photon processes (top dark green trace in Figure 8b and Figures S9–S12). The deviation of n from an integral number is a consequence of many factors, among which absorption of the upconverted emission and involvement of nonradiative decays in populating the emissive level are the most likely.^{5,22} However, linear two-step upconversion shares with nonlinear two-photon excitation fluorescence (TPEF) similar quadratic dependences for the emitted intensity with respect to incident pumping intensities,²³ and only the complete lack of upconverted signal observed for CrYCr upon laser excitation at 715 nm (dotted black trace in Figure 8a) excludes the operation of alternative ligand-centered or Cr(III)-centered TPEF mechanisms involving third-order nonlinear susceptibilities. The similar lack of Er-centered upconversion activity measured for GaErGa in the same conditions (black full trace in Figure 8a) eventually excludes competitive one ion ESA mechanisms, which are beyond the limit of detection in molecular complexes as reported by Reinhard and Güdel for nine-coordinate erbium(III) tris(dipicolinates).¹⁰ We safely conclude that indirect sensitization using two long-lived sensitizers and exploiting ETU mechanisms with a lanthanide activator in CrErCr indeed overcomes this limitation at the molecular level.

A rational analysis of the relative individual contributions of the Er-centered (red path) and the Cr-centered (green path) mechanisms to the upconverted emission in CrErCr (Figure 3a) required the synthesis of the second isostructural series of dinuclear dimetallic triple-stranded helicates [MLn(L2)]₃-(CF₃SO₃)₆ ($M = \text{Cr, Ga}$ and $\text{Ln} = \text{Y, Er}$) depicted in Figure 4b (Table S1, Appendix 2 in Supporting Information).²¹ For CrEr, ETU upconversion exclusively relies on the Er-centered mechanism (red path in Figure 2b), the efficiency of which is predicted to be statistically reduced by a factor $2^2 = 4$ with respect to CrErCr when all kinetic parameters and concentrations are identical. As designed by their molecular architectures (Figure S16), the electronic structures and photophysical properties of the CrN₆ and ErN₉ chromophores in CrEr (Figures S17–S20 and Tables S5 and S6) closely match those found in CrErCr (Figure 5 and Table S3 and S4), except for minor shifts in the energies of some excited states (Figures S21 and S22) resulting from the looser helical wrapping of the shorter strands in CrEr.¹⁹ However, minute energy change may significantly affect energy transfer processes, and we indeed observe a doubling of the Cr(²E) \rightarrow Er(⁴I_{9/2}) energy transfer rates in

CrEr ($W_1^{\text{Cr} \rightarrow \text{Er}} \approx 300\text{--}400 \text{ s}^{-1}$, eq 4 and Table S5), that may result from some level of improvement in the spectral overlap integral between the partners.¹⁹ Again, irradiation of GaEr and CrY in the NIR domain does not generate any upconverted emission, in line with negligible nonlinear TPEF response (CrY) and/or one ion ESA mechanisms (GaEr) operating in these dinuclear complexes. Though weaker than in CrErCr, NIR excitation into the sensitizer $\text{Cr}(^2\text{E}, ^2\text{T}_1 \leftarrow ^4\text{A}_2)$ transitions in CrEr also induce two-photon ($n = 1.67\text{--}1.79$) weak green upconverted $\text{Er}(^4\text{S}_{3/2} \rightarrow ^4\text{I}_{15/2})$ emission resulting from the Er-centered ETU mechanism (Figures 8 and S23–S25). The experimental intensity ratio of the upconverted emissions measured in the two complexes $I_{\text{Er}}^{\text{up}}(\text{CrErCr})/I_{\text{Er}}^{\text{up}}(\text{CrEr})$ evolves from 3 to 4 for pure solid-state samples to 7–8 in solution at low temperature (Figure 8b). Assuming that (i) the nonaccessible energy rate constants $W_2^{\text{Cr} \rightarrow \text{Er}}$ follow the trend found for $W_1^{\text{Cr} \rightarrow \text{Er}}$ (i.e., $W_1^{\text{Cr} \rightarrow \text{Er}}(\text{CrErCr}) = W_2^{\text{Cr} \rightarrow \text{Er}}(\text{CrErCr}) = 170 \text{ s}^{-1}$, $W_1^{\text{Cr} \rightarrow \text{Er}}(\text{CrEr}) = W_2^{\text{Cr} \rightarrow \text{Er}}(\text{CrEr}) = 295 \text{ s}^{-1}$ at 10K, Tables S3 and S5), (ii) the Cr-centered absorption cross section per metal are similar in CrEr and CrErCr complexes, and (iii) the concentrations are also similar for CrEr and CrErCr complexes, the model calculation predicts a ratio of $N^{\text{Er}(^4\text{S}_{3/2})}(\text{CrErCr})/N^{\text{Er}(^4\text{S}_{3/2})}(\text{CrEr}) \approx 300$ for the normalized steady-state population densities of the Er-centered excited level responsible for upconverted emission (Figure S26 and Appendix 1 in Supporting Information). The discrepancy with respect to $I_{\text{Er}}^{\text{up}}(\text{CrErCr})/I_{\text{Er}}^{\text{up}}(\text{CrEr}) \approx 8$ suggests that the experimentally nonaccessible parameters $W_2^{\text{Cr} \rightarrow \text{Er}}$ (rate of the second Cr \rightarrow Er energy transfer process) are indeed sufficiently different in the two complexes and specifically boost the Er-centered energy transfer upconversion process in the dinuclear complex. It is however worth remembering here that according to eq 6, $I_{\text{Er}}^{\text{up}}(\text{CrErCr})/I_{\text{Er}}^{\text{up}}(\text{CrEr})$ not only depends on the ratio of the steady-state populations $N^{\text{Er}(^4\text{S}_{3/2})}(\text{CrErCr})/N^{\text{Er}(^4\text{S}_{3/2})}(\text{CrEr})$ but also on $\phi_{\text{lum}}^{\text{Er}(^4\text{S}_{3/2})}(\text{CrErCr})/\phi_{\text{lum}}^{\text{Er}(^4\text{S}_{3/2})}(\text{CrEr})$, that is the ratio of the intrinsic quantum yields of the $\text{Er}(^4\text{S}_{3/2})$ level in the two complexes.¹⁹

$$\frac{I_{\text{Er}}^{\text{up}}(\text{CrErCr})}{I_{\text{Er}}^{\text{up}}(\text{CrEr})} = \frac{N^{\text{Er}(^4\text{S}_{3/2})}(\text{CrErCr})}{N^{\text{Er}(^4\text{S}_{3/2})}(\text{CrEr})} \cdot \frac{\phi_{\text{lum}}^{\text{Er}(^4\text{S}_{3/2})}(\text{CrErCr})}{\phi_{\text{lum}}^{\text{Er}(^4\text{S}_{3/2})}(\text{CrEr})} \quad (6)$$

Unfortunately, the $\text{Er}(^4\text{S}_{3/2} \rightarrow ^4\text{I}_{15/2})$ luminescence signal systematically appeared as a minor modulation of the underlying intense residual ligand-centered $\text{L2}(^1,^3\pi^* \rightarrow ^1\pi)$ transition in MErM (Figures 6a, S6, and S8) and MEr (Figure S18). We were therefore technically unable to obtain reliable lifetimes or quantum yields for the $\text{Er}(^4\text{S}_{3/2})$ level in these complexes, which prevented a definitive quantitative estimation of the additional contribution of the Cr-centered ETU mechanism in the trinuclear complex (green path in Figure 3a). In view of the fact that the Er cation is more accessible to external interactions in CrEr than in CrErCr (Figures 4 and S16), a considerable gain in intrinsic quantum yield in going from CrErCr to CrEr is, however, unlikely. On the contrary, a substantial variation of the second energy transfer rate constant due to minor changes in the spectral overlap integral between the emission spectrum of the $[\text{CrN}_6]$ chromophore and the transient absorption spectrum of the excited $[\text{ErN}_6]$ chromophore in CrEr^* and CrEr^*Cr^* are more realistic. An additional reason for the lower than expected intensity ratio is provided by the irradiation wavelength dependence of the upconversion intensity (Figure 7). Despite the smaller extinction coefficient of the $\text{Cr}(^2\text{T}_1 \leftarrow ^4\text{A}_2)$ transition compared to the one of the $\text{Cr}(^2\text{E} \leftarrow ^4\text{A}_2)$ transition it is more efficient in inducing upconversion. This is thought to be related to the homogeneous line

width of the transitions with respect to the inhomogeneous broadening. For the ^2E state at the working temperatures, the homogeneous line width of typically a few wavenumbers²⁴ is much smaller than the inhomogeneous width of around 250 cm^{-1} , whereas for the short-lived $^2\text{T}_1$ state the homogeneous line width is much larger. This effectively reduces the number of chromophores for which both chromium centers can be excited simultaneously by narrow band irradiation into the $\text{Cr}(^2\text{E} \leftarrow ^4\text{A}_2)$ absorption band.

CONCLUSION

The highly efficient nonradiative relaxation processes occurring in the erbium (supra)molecular coordination complexes GaErGa and GaEr prevent the detection of NIR to visible upconverted signals resulting from a one ion excited-state absorption (ESA) mechanism (Figure 1a). The introduction of a long-lived Cr(III) sensitizer in the CrEr complex improves this situation because of the intramolecular chromium-to-erbium communication which activates an alternative energy transfer upconversion (ETU) mechanism (red path in Figure 2b), which benefits from the larger absorption cross section of the sensitizer in the NIR and leads therefore to detectable upconverted green $\text{Er}(^4\text{S}_{3/2} \rightarrow ^4\text{I}_{15/2})$ emission. The connection of an additional Cr(III) sensitizer in CrErCr generates an alternative Cr-centered pathway for upconversion, in which two successive excitations are stored on the long-lived sensitizers prior to being transferred onto the activator to reach the target $\text{Er}(^4\text{I}_{3/2})$ emissive level (green path in Figure 3a). Statistically, in increments of one sensitizer unit in discrete Cr_nEr complexes, all rate constants, absorption cross sections and intrinsic quantum yields being equal, the kinetic models predict that the intensity of the quadratic response of the upconverted emission produced by the Er-centered ETU mechanism depends on n^2 (red path in Figure 3a) while that of the Cr-centered ETU mechanism increases as $n(n-1)$ (green path in Figure 3a). A nonstatistical gain in efficiency is therefore only expected between CrEr ($n=1$) and CrErCr ($n=2$) because of the abrupt implementation of the second mechanism (Figure 3b), a situation experimentally supported here with the observation of an increase of the upconverted emission by a factor of 7–8 in going from CrEr to CrErCr (a factor of 4 is predicted in absence of Cr-centered ETU mechanism). Predictions for a tetranuclear Cr_3Er system results in the creation of a pure statistical scheme with gains of 9/4 (red path, Er-centered ETU) and 6/2 (green path, Cr-centered ETU) with respect to CrErCr (Figure S27). This work demonstrates that lanthanide-centered light-upconversion can be induced at the molecular level and it might thus benefit from the high degree of rationalization, modeling and tuning provided by specific well-developed chemical toolboxes.

ASSOCIATED CONTENT

Supporting Information

Calculation of normalized steady-state population densities (Appendix 1), detailed experimental section (Appendix 2), determination of Jablonski diagrams (Appendix 3), kinetic scheme and matrices (Figures S1, S2, and S27), ^1H NMR (Figures S3 and S4), electronic absorption, excitation and emission spectra (Figures S5–S14, S17–S19, and S23–S25), Jablonski diagrams (Figures S20–S22), molecular structures (Figures S15 and S16) and computed normalized population densities (Figure S26), and tables collecting elemental analysis (Table S1), ESI-MS peaks (Table S2), and excited state lifetimes and energy transfer rate constants (Tables S3–S6). This material is available free of charge via the Internet at <http://pubs.acs.org>.

■ AUTHOR INFORMATION

Corresponding Authors

*E-mail: (A.H.) Andreas.Hauser@unige.ch.

*E-mail: (S.P.) Stephane.Petoud@cnrs-orleans.fr.

*E-mail: (C.P.) Claude.Piguet@unige.ch.

Author Contributions

[†]The first two authors contributed equally to this research work.

Notes

The authors declare no competing financial interest.

■ ACKNOWLEDGMENTS

This work was supported through grants from the Swiss National Science Foundation (Grant Numbers 200020_140222 and 200020_137567), the University of Geneva (INNOGAP), la Ligue contre le Cancer, and the Institut National de la Santé et de la Recherche Médicale (INSERM). The work was carried out within the COST Actions TD1004 and CM1006.

■ REFERENCES

- (1) (a) Monguzzi, A.; Tubino, R.; Hoseinkhani, S.; Campione, M.; Meinardi, F. Low Power, Non-Coherent Sensitized Photon Up-conversion: Modelling and Perspectives. *Phys. Chem. Chem. Phys.* **2012**, *14*, 4322–4332. (b) Kim, J.-H.; Deng, F.; Castellano, F. N.; Kim, J.-H. High Efficiency Low-Power Upconverting Soft Materials. *Chem. Mater.* **2012**, *24*, 2250–2252. (c) Huang, X.; Han, S.; Huang, W.; Liu, X. Enhancing Solar Cell Efficiency: the Search for Luminescent Materials as Spectra Converters. *Chem. Soc. Rev.* **2013**, *42*, 173–201.
- (2) Liu, Y.; Tu, D.; Zhu, H.; Chen, X. Lanthanide-doped Luminescent Nanoprobes: Controlled Synthesis, Optical Spectroscopy, and Bio-applications. *Chem. Soc. Rev.* **2013**, *42*, 6924–6958.
- (3) Bloembergen, N. Solid-state Infrared Quantum Counters. *Phys. Rev. Lett.* **1959**, *2*, 84–85.
- (4) Auzel, F. Upconversion and Anti-Stokes Processes with f and d Ions in Solids. *Chem. Rev.* **2004**, *104*, 139–173 and references therein.
- (5) Pollnau, M.; Gamelin, D. R.; Lüthi, S. R.; Güdel, H. U. Power Dependence of Upconversion Luminescence in Lanthanide and Transition-metal-ion Systems. *Phys. Rev.* **2000**, *B61*, 3337–3346.
- (6) $\lambda_p = 750$ nm has been selected for comparison purpose with the Cr/Er pairs, in which Cr(III) is irradiated in this energy range (see Figure S14).
- (7) Prudenzeno, F.; Mescia, L.; Allegratti, L.; Moizan, V.; Nazabal, V.; Smektala, F. Theoretical Study of Cascade Laser in Erbium-doped Chalcogenide Glass Fibers. *Opt. Mater.* **2010**, *33*, 241–245.
- (8) Georgescu, S.; Lupei, V. Q-switch Regime of 3 Micrometer Er:YAG Lasers. *IEEE J. Quantum Electron.* **1998**, *34*, 1031–1040.
- (9) Kumar, G. A.; Riman, R. E.; Torres, L. A. D.; Garcia, O. B.; Banerjee, S.; Kornienko, A.; Brennan, J. G. Chalcogenide-bound Erbium Complexes: Paradigm Molecules for Infrared Fluorescence Emission. *Chem. Mater.* **2005**, *17*, 5130–5135.
- (10) Reinhard, C.; Güdel, H. U. High-Resolution Optical Spectroscopy of $\text{Na}_3[\text{Ln}(\text{dpa})_3] \cdot 13\text{H}_2\text{O}$ with Ln = Er, Tm, Yb. *Inorg. Chem.* **2002**, *41*, 1048–1055.
- (11) van der Ende, B. M.; Aarts, L.; Meijerink, A. Lanthanide Ions as Spectral Converters for Solar Cells. *Phys. Chem. Chem. Phys.* **2009**, *11*, 11081–11095.
- (12) Pansare, V. J.; Hejazi, S.; Faenza, W. J.; Prud'homme, R. K. Review of Long-wavelength Optical and NIR Imaging Materials: Contrast Agents, Fluorophores, and Multifunctional Nanocarriers. *Chem. Mater.* **2012**, *24*, 812–827.
- (13) Wang, F.; Liu, X. Recent Advances in the Chemistry of Lanthanide-doped Upconversion Nanocrystals. *Chem. Soc. Rev.* **2009**, *38*, 976–989.
- (14) Haase, M.; Schäfer, H. Upconverting Nanoparticles. *Angew. Chem., Int. Ed.* **2011**, *50*, 5808–5829.
- (15) Aboshyan-Sorgho, L.; Cantuel, M.; Petoud, S.; Hauser, A.; Piguet, C. Optical Sensitization and Upconversion in Discrete Polynuclear Chromium-Lanthanide Complexes. *Coord. Chem. Rev.* **2012**, *256*, 1644–1663.
- (16) Ferraro, F.; Hadad, C. Z. Up-conversion and Migration by Energy Transfer: a Mixed Model for Doped Luminescent Solids. *J. Phys. Chem. C* **2012**, *116*, 7134–7143.
- (17) Blackburn, O. A.; Tropiano, M.; Sorensen, T. J.; Thom, J.; Beeby, A.; Bushby, L. M.; Parker, D.; Natrajan, L. S.; Faulkner, S. Luminescence and Upconversion from Thulium(III) Species in Solution. *Phys. Chem. Chem. Phys.* **2012**, *14*, 13378–13384 and references therein.
- (18) Aboshyan-Sorgho, L.; Besnard, C.; Pattison, P.; Kittilstved, K. R.; Aebischer, A.; Bünzli, J.-C. G.; Hauser, A.; Piguet, C. Near-infrared to Visible Light Upconversion in a Molecular Trinuclear d-f-d Complex. *Angew. Chem., Int. Ed.* **2011**, *50*, 4108–4112.
- (19) Aboshyan-Sorgho, L.; Nozary, H.; Aebischer, A.; Bünzli, J.-C. G.; Morgantini, P.-Y.; Kittilstved, K. R.; Hauser, A.; Eliseeva, S. V.; Petoud, S.; Piguet, C. Optimizing Millisecond Time Scale Near-infrared Emission in Polynuclear Chrome(III)-Lanthanide(III) Complexes. *J. Am. Chem. Soc.* **2012**, *134*, 12675–12684 and references therein.
- (20) Details for the X-ray crystal structure of $[\text{GaEr-Ga}(\text{L1})_3]_2(\text{CF}_3\text{SO}_3)_{18}(\text{C}_3\text{H}_5\text{N})_{30}$ will be published elsewhere. Figure S15 shows a superimposition of the molecular structures of CrEuCr and GaErGa.
- (21) Details for the X-ray crystal structure of $[\text{CrEr}(\text{L2})_3](\text{CF}_3\text{SO}_3)_6$ will be published elsewhere. Figure S16 shows a superimposition of the molecular structures of CrEr and CrYbCr.
- (22) (a) Gamelin, D. R.; Güdel, H. U. Design of Luminescent Inorganic Materials: New Photophysical Processes Studied by Optical Spectroscopy. *Acc. Chem. Res.* **2000**, *33*, 235–242. (b) Singh, A. K.; Rai, S. B.; Rai, D. K.; Singh, V. B. Upconversion and Thermometric Applications of Er(III)-doped Li:ReO₂ Glass. *Appl. Phys. B: Laser Opt.* **2006**, *82*, 289–294.
- (23) Andraud, C.; Maury, O. Lanthanide Complexes for Nonlinear Optics: from Fundamental Aspects to Applications. *Eur. J. Inorg. Chem.* **2009**, 4357–4371.
- (24) Riesen, H. Resonant Luminescence Line Narrowing of the R Lines in Tris(2,2'-bipyridine)rhodium Hexafluorophosphate Doped with Chromium $[\text{Rh}(\text{bpy})_3](\text{PF}_6)_3 \cdot \text{Cr}(\text{III})$. *J. Lumin.* **1992**, *54*, 71–78.